

Advanced imaging techniques: microscopy

Mona Golmohammadzadeh, Danielle L. Sexton, Shweta Parmar, and Elitza I. Tocheva*

Department of Microbiology and Immunology, Life Sciences Institute, Health Sciences Mall, The University of British Columbia, Vancouver, British Columbia, Canada

*Corresponding author: e-mail address: elitza.tocheva@ubc.ca

Contents

1. Introduction	2
2. Fluorescence light microscopy (fLM) and super-resolution light microscopy (srLM)	4
2.1 Single molecule localization microscopy (PALM/STORM)	6
2.2 Structured illumination microscopy (SIM)	8
2.3 Stimulated emission depletion microscopy (STED)	9
3. Cryo-electron microscopy (cryo-EM)	10
3.1 Single particle analysis (SPA)	11
3.2 Cryo-electron tomography (cryo-ET)	13
4. Conclusion	20
References	20

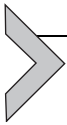
Abstract

For decades, bacteria were thought of as “bags” of enzymes, lacking organelles and significant subcellular structures. This stood in sharp contrast with eukaryotes, where intracellular compartmentalization and the role of large-scale order had been known for a long time. However, the emerging field of Bacterial Cell Biology has established that bacteria are in fact highly organized, with most macromolecular components having specific subcellular locations that can change depending on the cell’s physiological state (Barry & Gitai, 2011; Lenz & Søgaard-Andersen, 2011; Thanbichler & Shapiro, 2008). For example, we now know that many processes in bacteria are orchestrated by cytoskeletal proteins, which polymerize into surprisingly diverse superstructures, such as rings, sheets, and tread-milling rods (Pillhofer & Jensen, 2013). These superstructures connect individual proteins, macromolecular assemblies, and even two neighboring cells, to affect essential higher-order processes including cell division, DNA segregation, and motility. Understanding these processes requires resolving

the *in vivo* dynamics and ultrastructure at different functional stages of the cell, at macromolecular resolution and in 3-dimensions (3D). Fluorescence light microscopy (fLM) of tagged proteins is highly valuable for investigating protein localization and dynamics, and the resolution power of transmission electron microscopy (TEM) is required to elucidate the structure of macromolecular complexes *in vivo* and *in vitro*. This chapter summarizes the most recent advances in LM and TEM approaches that have revolutionized our knowledge and understanding of the microbial world.

Abbreviations

CLEM	correlative light and electron microscopy
cryo-EM	cryo-electron microscopy
cryo-ET	cryo-electron tomography
EM	electron microscopy
FIB	focused ion beam
fLM	fluorescence light microscopy
GFP	green fluorescent protein
LM	light microscopy
NA	numerical aperture
PAFP	photoactivatable fluorescent protein
PALM	photoactivated localization light microscopy
PSF	point spread function
SEM	scanning electron microscopy
SIM	structured illumination microscopy
SPA	single particle analysis
srLM	super resolution light microscopy
STED	stimulated emission depletion microscopy
STORM	stochastic optical reconstruction microscopy
T3SS	Type III secretion system
T6SS	Type VI secretion system
TEM	transmission electron microscopy



1. Introduction

The history of microscopy dates back to the 1590s with the creation of the first compound light microscope by the father-son duo Hans and Zacharias Jansen, who were Dutch eyeglass makers, and Hans Lippershey, another eyeglass maker. Their two-lens microscope represents the first major advancement in microscopy as it increased magnification compared to

previous single lens instruments. Subsequent developments were generated by the inventor Robert Hooke, who was gifted a three-lens microscope by his patron Robert Boyle (Lawson, 2016). Although the magnifying power was greater than preceding instruments, this microscope introduced chromatic and spherical aberrations. By adding a diaphragm, Hooke sharpened the light path and resolved these aberrations. Though this advancement led to another obstacle (the sample was now too dark to view), Hooke resolved it by adding a diffused light source comprised of an oil lamp positioned behind a flask of water. His initial microscopy findings on the fruiting bodies of molds, among other organisms, was published in *The Micrographia* in 1665, thus paving the way for others to keep improving and innovating microscopes. Pioneering work by his contemporary, Antonie van Leeuwenhoek, considered to be the “Father of Microbiology,” drastically increased the magnification of a single-lens microscope, thus allowing the first observation of microorganisms, now classified as bacteria, fungi and protists.

As cell biology advanced, so did the desire for higher magnification images. The development of the transmission electron microscope (TEM) in 1931 was a major step in that direction. The use of accelerated electrons as the illumination source enabled the investigation of denser objects and improved magnification of cellular features by more than 10^6 times. The beam path inside the TEM is maintained under a high vacuum to prevent scattering of electrons; however, this poses a problem for imaging biological samples since, under such conditions, their intracellular aqueous environment instantly evaporates. As a solution, in the 1950s, a chemical preservation method was developed, which relied on fixing, dehydrating, sectioning and staining biological samples, thus making them amenable to imaging with TEM (Dalton, 1952). While this major breakthrough advanced our understanding of biology for decades, numerous manipulations of the sample can cause significant alterations and loss of cellular ultrastructure. Thus, the desire to image cells in their native states has driven the improvement of sample preparation and imaging techniques ever since. This book chapter highlights some of the major technical advances in light and electron microscopy and provides examples of their applications to the field of microbiology (Fig. 1).

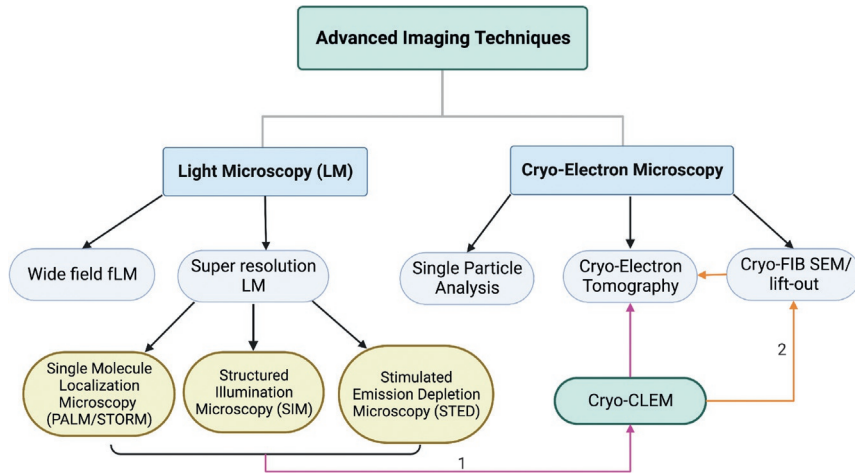
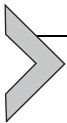


Fig. 1 Advanced imaging techniques. Light microscopy (LM) and electron microscopy (EM) approaches used to study microbial structure and function. Recent advances in LM include the development of super-resolution techniques that go beyond the diffraction limit of light. Cryo-preservation of biological samples has advanced EM applications. 1 and 2 outline two experimental workflows to study thin and thick samples, respectively. Created with [BioRender.com](https://www.biorender.com)



2. Fluorescence light microscopy (fLM) and super-resolution light microscopy (srLM)

Fluorescence as a biological phenomenon was first described in the 1800s. Fluorophores are molecules that absorb light of a specific wavelength, increase their energy levels through excitation, and subsequently release light of a longer wavelength when reverting to their lower energy states. The emission of light renders a color that can be seen with specialized microscopes, or even with the naked eye if in a large enough quantity. In 1962, aequorin, the protein responsible for the natural blue bioluminescence of the jellyfish *Aequorea victoria*, was identified (Shimomura, Johnson, & Saiga, 1962) and a decade later, the Green Fluorescent Protein (GFP) was isolated. The implementation of GFP and other fluorescent proteins as genetically-encoded markers revolutionized cell and molecular biology (Morise, Shimomura, Johnson, & Winant, 1974). The discovery and seminal nature of fluorescent proteins was awarded the 2008 Nobel Prize in Chemistry. Fluorescence light microscopy (fLM) aided numerous notable breakthroughs, one of which was that microorganisms possess organized

subcellular environments. Although the initial uses of the approach were focused on subcellular localization of proteins in fixed cells, fLM has since evolved to capture spatiotemporal dynamics and quantification in living cells (Gahlmann & Moerner, 2014).

The use of fLM has shaped our understanding of biological systems, especially when studying eukaryotic cells ($>10\ \mu\text{m}$), however, these approaches had limited applications for microbiology where the objects of interest are $<1\text{--}3\ \mu\text{m}$ in diameter. This is because the resolving power of fLM is related to the wavelength of light (λ) used for imaging and the numerical aperture (NA) of the imaging system. Since resolution is defined as $\lambda/(2 \times \text{NA})$, resolution of fLM is theoretically limited to $\sim 200\ \text{nm}$ in the lateral (x, y) and $\sim 500\ \text{nm}$ in the axial (z) planes. According to the Rayleigh criterion, in order for two distinct points to be considered resolved (or separate), the intensity of the two signals must have a 20% or greater difference between the maximum points of their intensity profiles. This means that objects that are closer than $\sim 200\text{--}300\ \text{nm}$ cannot be resolved by widefield (where the entire sample is exposed to a light source) fLM. This criterion presents a major problem in microbiology, since all of the internal structures of cells and their protein molecules are close together and smaller than $200\ \text{nm}$.

Recent advances in fLM that have focused on improving the resolution below the diffraction limit of light are referred to as super-resolution light microscopy (srLM) approaches. The first most accessible and widely-adopted technique for srLM is super-resolution confocal microscopy. Confocal imaging removes out-of-focus light by focusing a small beam of light at one narrow depth level at a time, allowing for optical sectioning of the sample and an improved signal-to-noise ratio. It utilizes traditional fluorophores and low laser intensities, which facilitate imaging and reduce sample damage, respectively. Furthermore, detector development has allowed for major gains in the resolution of confocal microscopy. Detector arrays enhance the spatial resolution to $\sim 120\ \text{nm}$ in the lateral plane and $350\ \text{nm}$ in the axial plane. New generation detectors are capable of spectral unmixing of up to 16 unique and overlapping fluorescence spectra, allowing for the use of a wider variety of fluorophores in multicolor imaging. Finally, low laser intensities and rapid image acquisition times enable visualization of dynamic processes in living cells. Thus, confocal microscopy is suited for imaging thicker samples, making it a superior approach for microbiologists studying host-pathogen interactions, tissue sections and biofilms. The principles and applications of some of the other major srLM techniques are described below (Fig. 2).

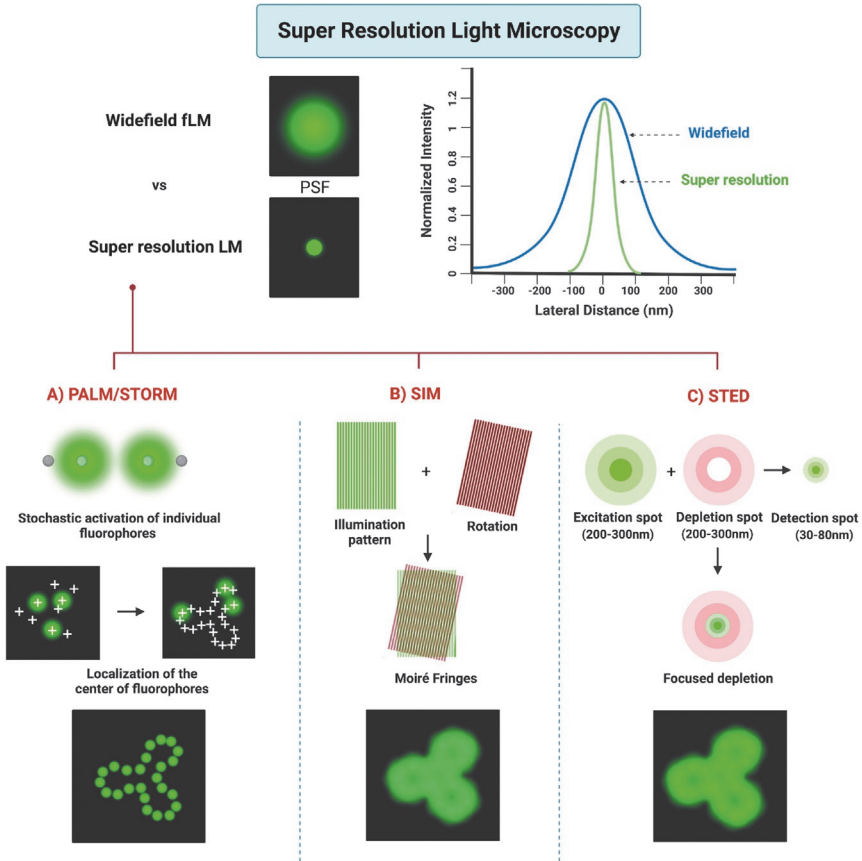


Fig. 2 Super-resolution light microscopy (srLM) techniques. The 3D diffraction pattern of light emitted from a fluorophore is referred to as the Point Spread Function (PSF). The PSF of widefield LM is much more diffuse compared to srLM approaches. Three main techniques of srLM are shown in A, B, and C. Fluorophores are depicted as circles, excitation light is represented as green, and depletion light is represented as red. See text for more detail. *Created with BioRender.com*

2.1 Single molecule localization microscopy (PALM/STORM)

Compared to confocal microscopy, more advanced srLM approaches involve the localization of individual fluorophores, the discovery of which was awarded the 2014 Nobel Prize in Chemistry. There are two major single molecule localization microscopy techniques—photoactivated localization light microscopy (PALM) (Betzig et al., 2006) and stochastic optical reconstruction microscopy (STORM) (Rust, Bates, & Zhuang, 2006),

both of which rely on the same basic principles (Fig. 2A). A small subset of fluorophores in the sample is stochastically activated one at a time over a long imaging period by using low energy activation laser. This generates a “blinking” event by each fluorophore, converting it from a bright to a dark state. In order to increase the resolution of the image, the light emitted from a fluorophore can be fit to a point spread function (PSF) using advanced mathematical models (Small & Stahlheber, 2014). Alternative models can also be applied, all of which can be computed using software such as ImageJ (Kirshner, Aguet, Sage, & Unser, 2013). Though the only true way to precisely localize and resolve a fluorophore is to use a PSF (Mortensen, Churchman, Spudich, & Flyvbjerg, 2010), often a Gaussian distribution is used to approximate the shape of the PSF, ultimately providing a 20-nm lateral and 50-nm axial resolution. A major distinction between the variety of single molecule localization microscopy techniques is the fluorophore being employed. For example, PALM utilizes genetically encoded photoactivatable fluorescent proteins (PAFP) such as PA-GFP, fused to a protein of interest, whereas STORM utilizes immunolabeling with antibodies fused to organic fluorophores. Both techniques can be done using commercially-available microscopes facilitating their applications in microbiology.

The first application of the single molecule localization microscopy was originally developed on a home-built microscope as a 2D imaging technique, and follow-up advances in image processing converted it into a 3D imaging modality (Huang, Wang, Bates, & Zhuang, 2008). As most biological specimens are thicker than the typical depth of focus (~800 nm) (Huang, Wang, et al., 2008), adjustments in data collection can be made. This is achieved by collecting images at different focal planes of a cell that are then stacked together to generate a 3D volume (Huang, Jones, Brandenburg, & Zhuang, 2008). Due to the long imaging times required to acquire a sufficient number of photons for imaging and difficulties in overlay precision, initial studies were performed using single fluorophores in fixed samples (Betzig et al., 2006; Hess, Girirajan, & Mason, 2006). Subsequent faster image acquisition allowed tracking the movement of molecules within cells, a major advantage for studying biological processes *in vivo*. The implementation of a variety of fluorophores has further permitted co-localization and visualization of the spatiotemporal dynamics of multiple proteins in living cells (Abdelsayed, Boukhatem, & Olivier, 2022; Gómez-García, Garbacik, Otterstrom, Garcia-Parajo, & Lakadamyali, 2018). Lastly, the improvement of lens technology is further increasing axial resolution and allowing for chromatic aberration correction at different light wavelengths.

Since the improved resolution of fLM is now able to distinguish between different forms of subcellular organization, mechanistic and structural studies are advancing our understanding of microbial systems. For instance, two-color PALM has been used to track the dynamics of cell division proteins in *Escherichia coli* and the archaeon *Haloferax volcanii* (Buss et al., 2015; Turkowyd et al., 2020). Organization of cytoskeletal elements in *Caulobacter crescentus* has also been investigated with multi-color PALM (Gahlmann et al., 2013). One prominent example of the importance of srLM involves determining the molecular mechanism behind bacterial chromosome segregation. Many bacteria, including *C. crescentus*, use partitioning (Par) systems to segregate their DNA, however, the exact mechanism for how these Par systems accomplish this is largely unknown. Different hypotheses exist, ranging from filamentous structures pulling the chromosome to a diffusion of the chromosome driven by a concentration gradient (Bouet, Ah-Seng, Benmeradi, & Lane, 2007; Fogel & Waldor, 2006; Hu, Vecchiarelli, Mizuuchi, Neuman, & Liu, 2017; Lim, Derman, & Pogliano, 2005; Lim et al., 2014). With widefield fLM, the Par system components were not resolved, making it difficult to support any of these hypotheses (Ptacin et al., 2010). Using PALM, however, researchers were able to resolve a retracting structure of ParA, an ATPase, also shown to form polymers *in vitro*. The ParA structure was observed proximal to the centromere-binding protein ParB, suggesting that ParA polymers are interacting with ParB and supporting a mechanism of filaments pulling the DNA (Ptacin et al., 2010).

2.2 Structured illumination microscopy (SIM)

Structured illumination microscopy (SIM) is another srLM approach that is conceptually different from the single molecule tracking approaches described above. SIM leverages the fluorescence of the sample through patterned gratings to achieve sub-diffraction resolution and relies heavily on a strong foundational understanding of physics and optics (Gustafsson, 2000; Gustafsson et al., 2008; Rainer Heintzmann & Christoph G. Cremer, 1999). Typically, an illumination pattern is applied to a sample labeled with up to three conventional fluorophores (genetically encoded or synthetic labels), resulting in regions of interference called Moiré fringes (Fig. 2B). Next, translations are applied to the illumination pattern and a set of images is collected at each rotation and translation. To determine the exact position of the fluorophore in real space, first the Fourier Transform (FT) of the PSF of the optical system is applied to the SIM frames and then reverse FT is used

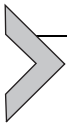
to computationally reconstructs a super-resolution image. The number of grating rotations can be increased to improve the image quality. SIM is quite computationally intensive and results in ~ 100 -nm lateral resolution with no substantial increase in axial resolution compared to widefield fLM. Utilizing z-stacks in combination with SIM imaging (3D SIM) increases the axial resolution to 300 nm (Kraus et al., 2017; Schermelleh et al., 2008). SIM is sensitive to out-of-focus light, which makes it useful only for samples thinner than ~ 30 μm . Though longer acquisition times have precluded SIM from imaging dynamic processes in live cells, newer imaging systems have faster acquisition times making the approach suitable for capturing cellular dynamics.

Several advances in microbiology have been made by using SIM and 3D SIM imaging. For example, researchers have been able to localize and structurally characterize proteins involved in cell division in *B. subtilis* (Eswaramoorthy et al., 2011). In order to trigger constriction, the protein FtsZ forms the septal Z-ring at the midpoint of dividing cells. Another player, DivIVA, is also essential during cell division, yet prior to the advent of super-resolution techniques, its role remained unclear (Hammond, White, & Eswara, 2019; Harry & Lewis, 2003). Imaging dividing *B. subtilis* cells with SIM revealed that DivIVA forms two flanking rings around the Z-ring. This observation led to the hypothesis that DivIVA flanks, and likely prevents, FtsZ from laying down more rings directly adjacent to the already forming septum. This discovery not only presented the higher order structure of DivIVA, but it also provided insight into possible mechanisms guiding cellular division in rod-shaped bacteria.

2.3 Stimulated emission depletion microscopy (STED)

To achieve super-resolution, STED relies on the use of two laser pulses and patterned illumination of the sample (Hell & Wichmann, 1994) (Fig. 2C). The fluorophores in the sample are excited by the first laser pulse, while a second laser pulse, typically in a torus shape, is used to deplete the emission of fluorophores in all areas except the center of the beam. This depletion spatially limits the region emitting fluorescence to the center of the field of view and allows fluorophores in close proximity to be distinguished, resulting in ~ 50 nm resolution. In newer instruments, the STED laser is circularly polarized to achieve super-resolution along the axial plane. Improvements in detectors are increasing imaging speed and enabling visualization of up to five fluorophores. The net result is that the dynamics of several fluorophores can be visualized at 30-nm lateral and 100-nm axial

resolution. Spectral deconvolution is also being adapted for use in STED microscopy to separate emission from spectrally-overlapping fluorophores. As with PALM/STORM and SIM, the resolution of STED worsens with increasing sample thickness. While STED hardware has been complicated to use in the past, the technology is maturing and newer instruments show promise for future microbiology applications. For example, STED has been used to monitor peptidoglycan synthesis in conjunction with new generation fluorescent D-amino acids in a variety of monoderm and diderm bacteria (Söderström, Ruda, Widmalm, & Daley, 2020).



3. Cryo-electron microscopy (cryo-EM)

To determine the structure of cells and macromolecular complexes, the high resolving power of TEM is indispensable. Cryo-EM is a technique that applies TEM to cryogenically preserved biological samples (kept at -170°C), and produces 3D reconstructions. In the 1980s, Dubochet and colleagues discovered that if biological samples are frozen fast enough ($>10^6$ $^{\circ}\text{C/s}$), the surrounding water molecules form amorphous ice rather than crystalline ice (Dubochet et al., 1988). The amorphous (also known as vitreous) ice is compatible with TEM imaging since it appears as “glass-like” and does not interfere with the visualization of cellular structures. In addition, cryo-preservation ensures simultaneous immobilization of all macromolecular components in their native states. Since many protein networks are sensitive to osmotic or temperature changes, cryo-preservation minimizes artifacts and opens new doors to study biological samples at unprecedented resolution. The significance of cryo-EM and its contributions to medicine were recognized in 2017 when Dubochet, Frank and Henderson were awarded the Nobel Prize in Chemistry for pioneering the technique.

There are two major cryo-EM modalities that are nowadays used routinely to study proteins and cellular structures (Fig. 3). The first, single particle analysis (SPA), focuses on imaging macromolecular complexes *in vitro*, and the second, cryo-electron tomography (cryo-ET), is focused on imaging intact cells. Both techniques generate 3D structures in near-native states, leverage cryo-preservation and rely on the same TEM instrument and software for imaging. Thus, developments in imaging hardware and software impact both modalities. More details about SPA and cryo-ET are discussed in the sections below.

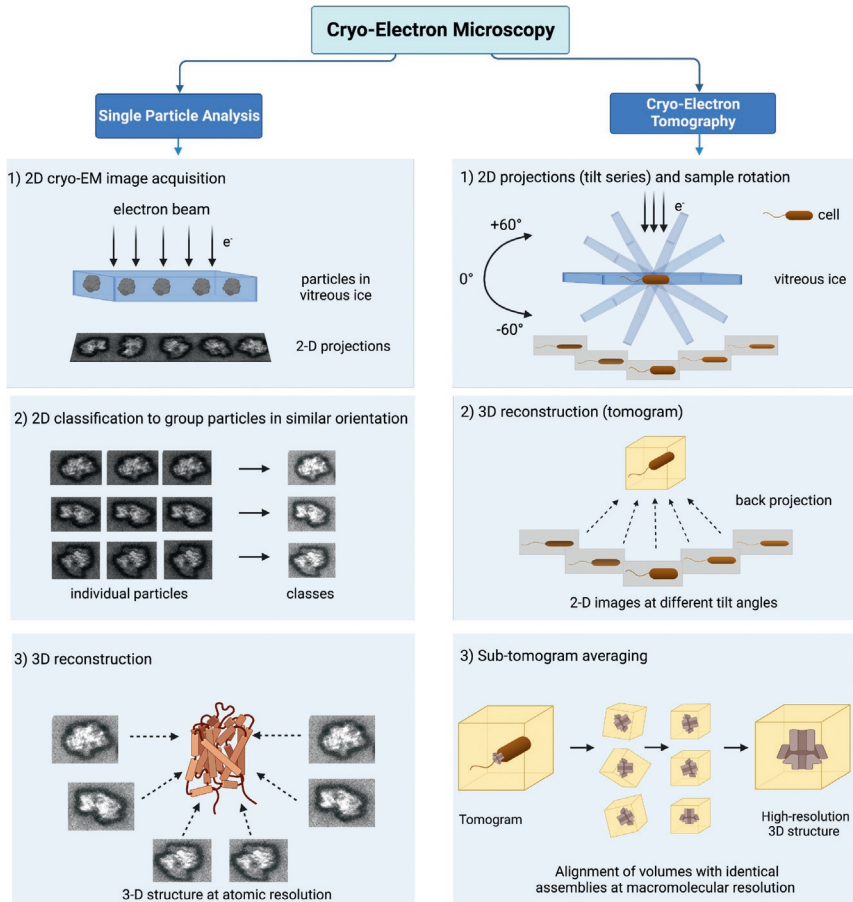


Fig. 3 Cryo-electron microscopy techniques. Single Particle Analysis: (1) Vitrified samples are imaged in a single plane in the TEM, producing 2D projections. (2) Multiple 2D projections are taken and then grouped into classes based on the particle orientations. (3) The classes are then aligned and reconstructed to form a 3D volume to an atomic resolution. Cryo-electron tomography: (1) The vitrified sample is rotated inside the electron microscope while 2D projections are collected. (2) The 2D projections are then reconstructed to yield a tomogram. (3) Sub-tomogram averaging is an optional step that averages multiple sub-tomographic volumes to increase the signal-to-noise ratio and improve the resolution of a 3D macromolecular complex. *Created with BioRender.com*

3.1 Single particle analysis (SPA)

SPA is a powerful method for protein structure determination that relies on collecting thousands of micrographs of purified proteins or macromolecular complexes. The sample is frozen on EM grids and, due to the large number

and varied orientations of the particles, the collected 2D projection images can be used to generate a 3D volume (Fig. 3A). SPA has many advantages in comparison to X-ray crystallography, the historically used method for atomic structure determination. For example, the access and accuracy of X-ray crystallography is highly dependent on the ability of biological molecules to form crystals that diffract to high resolution. Limited by the molecule size and characteristics such as hydrophobicity and dynamic regions, the structures of many proteins, including membrane proteins, were thus not amenable to the technique. SPA overcomes several of these limitations and has been particularly instrumental for the study of membrane proteins, protein complexes, and macromolecular machines such as viruses, ribosomes, and proteasomes (Doyle et al., 2022; Sun et al., 2020; Yuan et al., 2018).

Recent developments in data acquisition and processing have resulted in major advances in the field where structures solved using SPA can now reach atomic resolution (Nakane et al., 2020). During data processing, same structures are organized into 2D classes where views representing the same class are averaged to increase the signal-to-noise ratio. Then, a 3D reconstruction is calculated and depending on the resolution, amino acid side chains can be identified. Furthermore, 3D refinement may reveal conformational and compositional heterogeneity providing valuable insight into structural and functional intermediates (Su et al., 2021). Structural prediction software, such as AlphaFold (Jumper et al., 2021) and RosettaFold (Baek et al., 2021), are also aiding in structural determination as predicted structures using these methods can be fit into low resolution SPA volumes to clarify the positions of proteins within a complex.

SPA has led to major advances in microbiology, specifically in the field of membrane-bound proteins (Fig. 4). For example, bacteria possess specialized secretion systems that are membrane-associated nanomachines and aid in transporting molecules in and out of cells. They promote pathogenesis by secreting virulence factors (substrates) that are required for intracellular survival and evading the bactericidal mechanisms of host cells. SPA has become an invaluable approach to study the structure and function of the types I-IV, VI, VII and IX systems and has led to major advances in understanding their mechanisms. One of the best studied examples is the Type III secretion system (T3SS, also called injectosome, Fig. 4A), which is used by Gram-negative bacteria to secrete virulence factors across their inner and outer membranes, as well as across the plasma membrane of the host. The T3SS has a characteristic needle component (the translocon) that was previously hypothesized to transport the substrates. Using SPA, researchers were able to solve

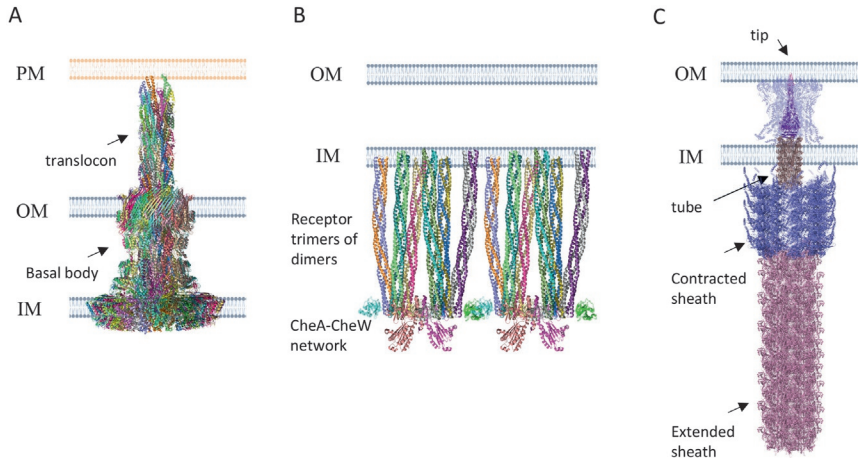


Fig. 4 Atomic models of membrane-bound macromolecular complexes in bacteria. (A) The T3SS from *Salmonella typhimurium*, composed of the basal body and translocon, secretes virulence factors across the bacterial inner membrane (IM), outer membrane (OM), and host cell plasma membrane (PM). (B) Chemoreceptor arrays are trimers of dimers spanning the IM and relaying signal from the periplasm into the cell via the CheA (histidine kinase) and CheW (coupling protein). (C) The T6SS found in *Myxococcus xanthus* is a membrane-associated intracellular contractile injection system. It is composed of the sheath protein VipA, tube, and tip. Created with [BioRender.com](https://www.biorender.com).

the complex to subnanometer resolution and identify the main proteins comprising the system and determine their stoichiometry. By tagging a putative substrate, SPA studies were further able to visualize it “trapped” inside the translocon of the T3SS, lending strong support for the mode of secretion (Radics, Königsmaier, & Marlovits, 2014). The T3SS-mediated secretion is now described as trapping unfolded substrates and passing them through the lumen of translocon. Structural studies further showed that the 15-Å lumen, as well as the outer membrane secretin component, limit the size of substrates passing through the system (Hu et al., 2018).

3.2 Cryo-electron tomography (cryo-ET)

Similar to SPA, cryo-ET generates 3D reconstructions, however the technique has the unique capacity to resolve structures directly within cells. To prepare the sample for data collection, a few microliters of a bacterial culture are applied to an EM grid and rapidly frozen in order to preserve the intracellular environment and prevent the formation of crystalline ice. Inside the TEM, tilt series of each cell/target are collected by continuously rotating the sample while taking 2D micrographs (Fig. 3B). 3D volumes, or tomograms,

are then reconstructed using backprojection computational methods. By providing macromolecular (~ 3 nm) resolution, cryo-ET reveals the native structure of complexes and their interactions with other cellular components.

Cryo-ET has been used to characterize numerous macromolecular assemblies in bacteria, as well as study essential cellular processes. For example, this approach was used to directly visualize the interaction of the T3SS of *Salmonella typhimurium* with host cells. As described above, the T3SS is used to secrete substrates into the host that lead to actin polymerization, membrane ruffling and engulfment of the pathogenic bacteria (Coburn, Sekirov, & Finlay, 2007). By using a combination of deletion mutants and fusion proteins, all of the components of the export apparatus, as well as the cytoplasmic platform that is essential for sorting the needle subunits and substrates, were identified (Park et al., 2018). Visualizing host-pathogen interactions directly further showed how the tip of the translocon binds to the plasma membrane of eukaryotic cells and mediates signal transduction, providing the most detailed view of a secretion system in its cellular context to date. Application of cryo-ET to other systems will undoubtedly provide similar structural and functional insights for other systems.

3.2.1 Subtomogram averaging

To improve the resolution of cryo-ET, identical structures within a cell (or repeating structures among cells) can be computationally superimposed and averaged. This approach, termed “subtomogram averaging,” capitalizes on the advantages of cryo-ET, while applying the principles of SPA (Fig. 3B). Here, each structure of interest is extracted from the raw tilt series to undergo 3D averaging and refinement (Bharat & Scheres, 2016; Scaramuzza & Castaño-Díez, 2021). As a result, similar to SPA, higher signal-to-noise ratio improves the resolution to subnanometer and reduces missing data artifacts. Subtomogram averaging has been particularly beneficial for structures that are abundant *in vivo* and thus readily observable, such as chemoreceptor arrays, flagellar motors, secretion systems, and surface layers (S-layers) (Chen et al., 2011; Martinez et al., 2022; von Kügelgen et al., 2020). Although the resolution of structures obtained by subtomogram averaging is not comparable to that of SPA, a major advantage of this approach is the ability to localize macromolecular assemblies *in situ* (Ferreira et al., 2019). For example, a novel component of yet unknown function was recently discovered in association with the inner membrane of the flagellar T3SS in several Gram-negative bacteria (Kaplan et al., 2022), thus identifying new areas for future research.

Data collection for subtomogram averaging presents several challenges, particularly pertaining to structures that are sensitive to the electron beam. In cryo-ET, the highest resolution images are taken at the beginning of a tilt series, prior to accumulation of electron damage, whereas images taken at higher tilt angles are noisier due to the increased sample thickness and electron scattering (Hagen, Wan, & Briggs, 2017). To accelerate data acquisition and in turn minimize overall exposure of the sample to the electron beam, tilt increments can be increased, and the total tilt angles can be reduced. Additionally, modified tilt schemes can improve the resolution by further reducing electron damage at the lower tilts when the sample is thinnest (Hagen et al., 2017). Major advances are to be made in software development for subtomogram averaging. Currently, data processing relies on a variety of unintegrated software tools, necessitating homemade workarounds due to compatibility issues. Recently, machine learning based particle selection has been developed in some software pipelines (Scaramuzza & Castaño-Díez, 2021). Similar to SPA, the algorithm can be trained on a subset of particles for subsequent automatic selection of targets in tomograms. More sophisticated 3D heterogeneous refinement tools are also making their way into subtomogram averaging. These tools allow for higher resolution structures to be obtained through distinguishing different conformations of the same complex (Himes & Zhang, 2018).

Atomic structures generated by higher resolution methods, such as X-ray crystallography or SPA can be used in conjunction with subtomogram averaging to generate a pseudoatomic model of macromolecular assemblies as they appear *in vivo*. This approach has been successfully applied to study the bacterial chemoreceptor arrays (Briegel et al., 2012; Muok et al., 2020; Yang et al., 2019). Chemoreceptors are transmembrane complexes that direct the movement of cells to and away from chemicals in the environment. Subtomogram averaging revealed that receptors formed extended hexagonal lattices composed of trimers of dimers. By fitting the crystal structures of individual receptors into the EM maps, a detailed network of interactions among subunits was identified. The structural connections have provided a model that can explain the cooperative behavior and signal transduction during chemotaxis (Fig. 4B).

3.2.2 Correlative light and electron microscopy (CLEM)

Identifying objects within the crowded environment of the cell is limited by our knowledge of complexes *in vivo*. The most powerful method to identify objects of interest in cells for subsequent imaging with cryo-ET is CLEM.

In this approach, proteins of interest are fused to fluorophores and coarsely localized using fLM. The fLM images are then used to identify targets for subsequent cryo-ET analysis of the same sample. CLEM approaches aid in the identification of subcellular structures and further bridge the resolution gap between different imaging modalities.

Although powerful, CLEM approaches have limitations: fLM is best carried out at room temperature using oil-immersion lenses with high numerical aperture (NA \sim 1.4). Under these conditions, even slight cellular movement can prevent subsequent correlation with cryo-ET. As a result, only relatively static structures such as bacterial stalk cross-bands or eukaryotic focal adhesions have been studied (Medalia & Geiger, 2010; Sartori et al., 2007; Schlimpert et al., 2012). Alternatively, cells can be chemically fixed before imaging, however, fixation can introduce artifacts and destroy intracellular features such as cytoskeletal filaments (Lippincott-Schwartz & Manley, 2009; Schnell, Dijk, Sjollem, & Giepmans, 2012; Whelan & Bell, 2015). For best results, prior to fLM imaging, cells should be cryogenically preserved. Since imaging needs to be carried out under liquid nitrogen, the use of long-working distance air objectives (low NA of \sim 0.7) severely limit the resolution of cryo-fLM.

A major improvement in CLEM approaches is the implementation of srLM under cryogenic conditions. For example, cryo-PALM was successfully applied to frozen *Myxococcus xanthus* cells to identify multiple and new conformations of the Type VI secretion system (T6SS). The T6SS is a membrane-associated intracellular contractile injection system that plays a role in interbacterial competition and competence (Fig. 4C) (Cherrak, Flaugnatti, Durand, Journet, & Cascales, 2019). By tagging the sheath protein VipA with a PA-GFP, extended and contracted conformations were observed in tomograms, corresponding to loaded and fired states of the system (Chang et al., 2014). Cryo-PALM is a powerful technique; however, it requires the use of home-built instruments and photo-activatable fluorophores that have prevented its routine application in microbiology.

Nowadays, commercially available cryo-srLM instruments provide a good balance between ease of use, rapid data collection, and image quality. Software plugins can automatically correlate images from different magnifications, facilitating downstream correlation with other imaging modalities.

3.2.3 Cryo-focused ion beam (Cryo-FIB) milling and lift-out

Due to the limiting penetrative power of electrons, samples thicker than 500nm are not amenable for direct imaging with cryo-ET. Cryo-FIB milling is an approach that produces 100–300nm thin sections, (lamellae) that

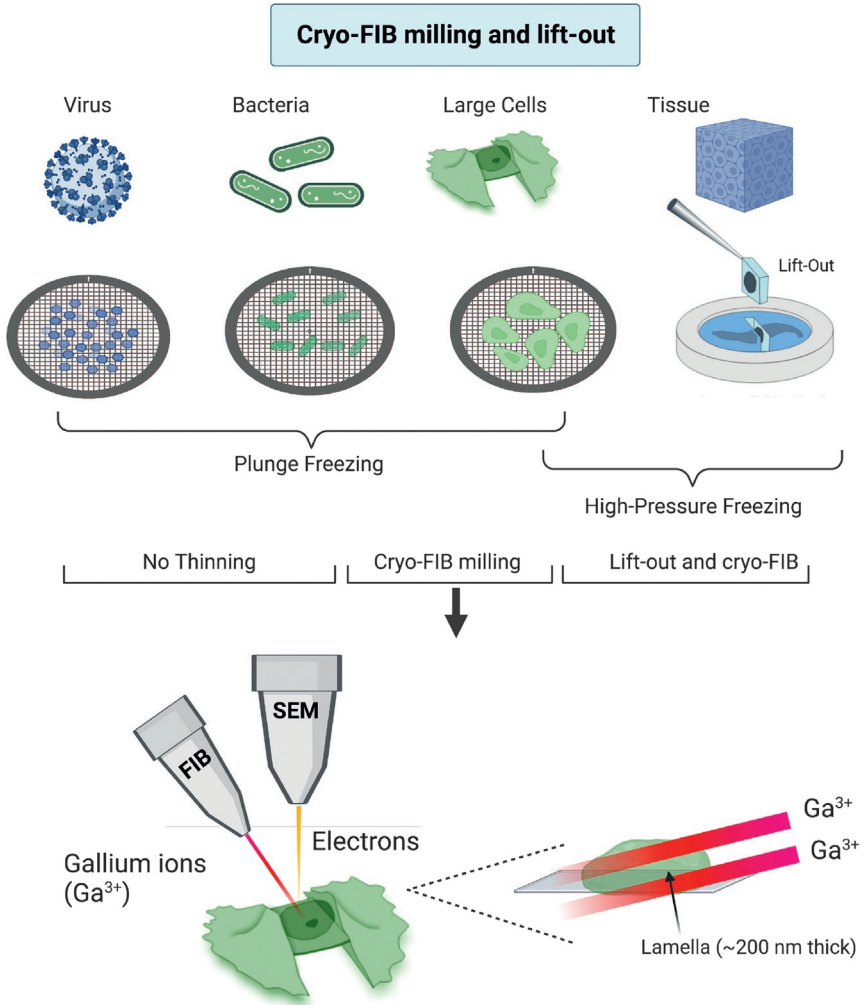


Fig. 5 Cryo-FIB milling and lift-out overview. Plunge freezing is used to vitrify samples, such as viruses and bacteria that are less than $10\ \mu\text{m}$ thick, directly onto EM grids. For thicker samples, cryo-FIB milling is used to produce thin ($\sim 200\ \text{nm}$) sections called lamellae that can be imaged using cryo-ET. Gallium ions are used during FIB milling to ablate excess material. An electron beam is also used to monitor the milling process with scanning electron microscopy (SEM). Tissue samples can be frozen using high-pressure and a section can be removed using the lift-out approach. The section is then placed on an EM grid and further milled using cryo-FIB before imaging with cryo-ET. Created with [BioRender.com](https://www.biorender.com)

can subsequently be imaged with cryo-ET (Fig. 5). The initial stages of sample preparation are similar to those for cryo-ET, allowing for seamless integration of the two methods into the same workflow. After plunge-freezing on a cryo-EM grid, the sample is transferred to a cryo-FIB instrument for

cryo-FIB milling. Here a beam of high energy gallium (Ga^{3+}) ions is used to ablate material and produce lamellae. Cryo-FIB instruments typically have two beams, one for milling (Ga^{3+}) and the other (electrons) for visualizing the sample with scanning EM (SEM). SEM helps monitor the milling process as it is occurring and can further generate volume data for 3D analysis (Hsieh, Schmelzer, Kishchenko, Wagenknecht, & Marko, 2014; Mahamid et al., 2015; Medeiros, Böck, & Pilhofer, 2018; Zachs et al., 2020).

Cryo-FIB milling has made it possible to visualize thick bacterial samples to unprecedented detail. For instance, the cell division machinery during endospore formation in *B. subtilis* was found to localize exclusively to the mother cell side of the forming septum (Khanna, Lopez-Garrido, Sugie, Pogliano, & Villa, 2021). This is in contrast to vegetative septa where the cell division machinery localizes to both sides of the developing septum. This approach is also an essential tool for researchers interested in the structural biology of host-pathogen interactions. While the T3SS has been extensively characterized using both SPA and cryo-ET, it is challenging to directly image the structure of the secretion system during the infection process due to sample thickness. Using cryo-FIB milling, cryo-ET, and SPA, the structure of the injectosome of *Yersinia enterocolitica* was studied inside the phagosome of infected human cells. The unprecedented images revealed that the T3SS formed direct contact with the phagosomal membrane and provided insight into the structural differences of the injectosome compared to other bacteria (Berger et al., 2021). Such applications pave the way for future 3D studies of infection-relevant protein complexes in host-pathogen interactions.

For samples thicker than $50\ \mu\text{m}$, such as biofilms and tissue, an *in situ* lift-out method has been developed under cryogenic conditions (Schaffer et al., 2019). This approach is routinely used for manipulating materials at room temperature, however, its implementation under cryogenic conditions is now allowing us to apply it to biological systems. In the cryo-lift-out method, the thick biological sample is first vitrified using high-pressure freezing. Next, a small volume is extracted using a mechanical micromanipulator kept at a temperature below $-145\ ^\circ\text{C}$ to maintain the sample in a vitreous state. The volume of interest is then transferred onto an EM grid for final cryo-FIB thinning before being imaged with cryo-ET (Schaffer et al., 2019).

3.2.4 Super-resolution cryo-CLEM, cryo-FIB and cryo-ET of bacterial cells

Depending on the biological question, the approaches described in this chapter can be combined in numerous ways and applied to a variety of

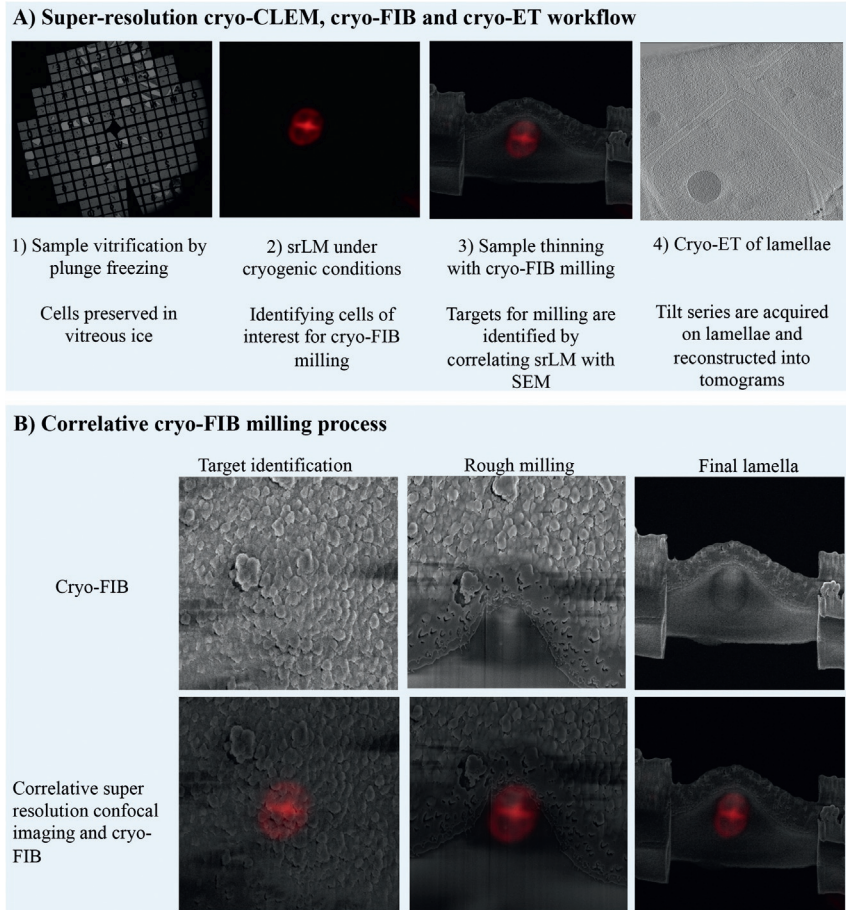


Fig. 6 Integrated super-resolution cryo-CLEM, cryo-FIB and cryo-ET to study the bacterial cell envelope. (A) Correlative cryo-FIB milling and cryo-ET workflow. *Deinococcus radiodurans* cells were plunge frozen on EM grids and srLM under cryogenic conditions was used to identify targets for cryo-FIB milling. Cryo-FIB milling was monitored using SEM. Tomograms of final lamellae were collected using cryo-ET. (B) Major steps during target identification and correlation between cryo-srLM and cryo-FIB. Adapted from Sexton, D. L., Burgold, S., Schertel, A., & Tocheva, E. I. (2022). Super-resolution confocal cryo-CLEM with cryo-FIB milling for in situ imaging of *Deinococcus radiodurans*. Current Research in Structural Biology, 4, 1–9.

systems. For example, a super-resolution cryo-CLEM and cryo-FIB-SEM volume imaging approach was recently applied to structurally characterize the cell envelope of dividing *Deinococcus radiodurans* bacterial cells (Fig. 6). *D. radiodurans* is a radiation-resistant bacterium with unique structural and

functional properties. The bacterium is known to have a unique cell envelope with an outer membrane that lacks the typical lipopolysaccharide (LPS) lipids, and has a surface S-layer composed of multiple protein complexes (Farci et al., 2021). The extreme resistance of the *D. radiodurans* cells to UV light and desiccation has been attributed to the cell envelope and in particular the S-layer (Farci, Slavov, Tramontano, & Piano, 2016). Due to its size ($>4\ \mu\text{m}$ in diameter), direct imaging of *D. radiodurans* with cryo-ET has not been feasible to date. By applying a combination of advanced imaging approaches, the native *in vivo* structure of the cell envelope revealed the presence of a thick layer of peptidoglycan, a novel tethering system composed of OmpM, and the organization of the S-layer in a hexagonal lattice (Kügelgen et al., 2022; Sexton, Burgold, Schertel, & Tocheva, 2022). Furthermore, cytoskeletal filaments, FtsA and FtsZ, were observed at the leading edges of constricting septa and numerous, previously uncharacterized, macromolecular complexes were found associated with the cytoplasmic side of the inner membrane (Sexton et al., 2022).



4. Conclusion

Combining advanced imaging techniques with extensive biochemical and molecular biology approaches will open new lines of investigation into the physiology and evolution of bacteria. Imaging hardware, automation software to guide image collection, and machine learning tools are pushing imaging forward. Gains need to be made in the areas of automated feature detection, axial resolution of super-resolution techniques, particularly under cryogenic conditions, and improving data processing so that more could be done with smaller datasets. Much needed advances include identifying macromolecular complexes in cryo-ET without the labelling of proteins of interests, and performing SPA on proteins that are less abundant in the cell, without the need for extremely large datasets. Microscopy advancements continue as we reach new levels of sight.

References

- Abdelsayed, V., Boukhatem, H., & Olivier, N. (2022). An optimized buffer for repeatable multicolor STORM. *ACS Photonics*. <https://doi.org/10.1021/acsp Photonics.2c01249>.
- Baek, M., DiMaio, F., Anishchenko, I., Dauparas, J., Ovchinnikov, S., Lee, G. R., et al. (2021). Accurate prediction of protein structures and interactions using a three-track neural network. *Science*, *373*(6557), 871–876. <https://doi.org/10.1126/science.abj8754>.
- Barry, R., & Gitai, Z. (2011). Self-assembling enzymes and the origins of the cytoskeleton. *Current Opinion in Microbiology*, *14*(6), 704–711. <https://doi.org/10.1016/j.mib.2011.09.015>.

- Berger, C., Ravelli, R. B. G., López-Iglesias, C., Kudryashev, M., Diepold, A., & Peters, P. J. (2021). Structure of the *Yersinia* injectisome in intracellular host cell phagosomes revealed by cryo FIB electron tomography. *Journal of Structural Biology*, 213(1), 107701. <https://doi.org/10.1016/j.jsb.2021.107701>.
- Betzig, E., Patterson, G. H., Sougrat, R., Lindwasser, O. W., Olenych, S., Bonifacino, J. S., et al. (2006). Imaging intracellular fluorescent proteins at nanometer resolution. *Science*, 313(5793), 1642–1645. <https://doi.org/10.1126/science.1127344>.
- Bharat, T. A. M., & Scheres, S. H. W. (2016). Resolving macromolecular structures from electron cryo-tomography data using subtomogram averaging in RELION. *Nature Protocols*, 11(11), 2054–2065. <https://doi.org/10.1038/nprot.2016.124>.
- Bouet, J.-Y., Ah-Seng, Y., Benmeradi, N., & Lane, D. (2007). Polymerization of SopA partition ATPase: Regulation by DNA binding and SopB. *Molecular Microbiology*, 63(2), 468–481. <https://doi.org/10.1111/j.1365-2958.2006.05537.x>.
- Briegel, A., Li, X., Bilwes, A. M., Hughes, K. T., Jensen, G. J., & Crane, B. R. (2012). Bacterial chemoreceptor arrays are hexagonally packed trimers of receptor dimers networked by rings of kinase and coupling proteins. *Proceedings of the National Academy of Sciences*, 109(10), 3766–3771. <https://doi.org/10.1073/pnas.1115719109>.
- Buss, J., Coltharp, C., Shtengel, G., Yang, X., Hess, H., & Xiao, J. (2015). A multi-layered protein network stabilizes the *Escherichia coli* FtsZ-ring and modulates constriction dynamics. *PLoS Genetics*, 11(4), e1005128. <https://doi.org/10.1371/journal.pgen.1005128>.
- Chang, Y.-W., Chen, S., Tocheva, E. I., Treuner-Lange, A., Löbach, S., Søgaard-Andersen, L., et al. (2014). Correlated cryogenic photoactivated localization microscopy and cryo-electron tomography. *Nature Methods*, 11(7), 737–739. <https://doi.org/10.1038/nmeth.2961>.
- Chen, S., Beeby, M., Murphy, G. E., Leadbetter, J. R., Hendrixson, D. R., Briegel, A., et al. (2011). Structural diversity of bacterial flagellar motors. *The EMBO Journal*, 30(14), 2972–2981. <https://doi.org/10.1038/emboj.2011.186>.
- Cherrak, Y., Flaugnatti, N., Durand, E., Jourmet, L., & Cascales, E. (2019). Structure and activity of the type VI secretion system. *Microbiology Spectrum*, 7(4), 7.4.11. <https://doi.org/10.1128/microbiolspec.PSIB-0031-2019>.
- Coburn, B., Sekirov, I., & Finlay, B. B. (2007). Type III secretion systems and disease. *Clinical Microbiology Reviews*, 20(4), 535–549. <https://doi.org/10.1128/CMR.00013-07>.
- Dalton, A. J. (1952). A study of the Golgi material of hepatic and intestinal epithelial cells with the electron microscope. *Zeitschrift für Zellforschung und Mikroskopische Anatomie*, 36(6), 522–540. <https://doi.org/10.1007/BF00347683>.
- Doyle, M. T., Jimah, J. R., Dowdy, T., Ohlemacher, S. I., Larion, M., Hinshaw, J. E., et al. (2022). Cryo-EM structures reveal multiple stages of bacterial outer membrane protein folding. *Cell*, 185(7), 1143–1156.e13. <https://doi.org/10.1016/j.cell.2022.02.016>.
- Dubochet, J., Adrian, M., Chang, J.-J., Homo, J.-C., Lepault, J., McDowell, A. W., et al. (1988). Cryo-electron microscopy of vitrified specimens. *Quarterly Reviews of Biophysics*, 21(2), 129–228. <https://doi.org/10.1017/S0033583500004297>.
- Eswaramoorthy, P., Erb, M. L., Gregory, J. A., Silverman, J., Pogliano, K., Pogliano, J., et al. (2011). Cellular architecture mediates DivIVA ultrastructure and regulates min activity in *Bacillus subtilis*. *MBio*, 2(6). <https://doi.org/10.1128/mBio.00257-11>. e00257-11.
- Farci, D., Kereiche, S., Pangeni, S., Haniewicz, P., Bodrenko, I. V., Ceccarelli, M., et al. (2021). Structural analysis of the architecture and *in situ* localization of the main S-layer complex in *Deinococcus radiodurans*. *Structure*, 29(11), 1279–1285.e3. <https://doi.org/10.1016/j.str.2021.06.014>.
- Farci, D., Slavov, C., Tramontano, E., & Piano, D. (2016). The S-layer protein DR_2577 binds deinoxanthin and under desiccation conditions protects against UV-radiation in *Deinococcus radiodurans*. *Frontiers in Microbiology*, 7. <https://www.frontiersin.org/articles/10.3389/fmicb.2016.00155/full>.

- Ferreira, J. L., Gao, F. Z., Rossmann, F. M., Nans, A., Brenzinger, S., Hosseini, R., et al. (2019). γ -proteobacteria eject their polar flagella under nutrient depletion, retaining flagellar motor relic structures. *PLoS Biology*, 17(3), e3000165. <https://doi.org/10.1371/journal.pbio.3000165>.
- Fogel, M. A., & Waldor, M. K. (2006). A dynamic, mitotic-like mechanism for bacterial chromosome segregation. *Genes & Development*, 20(23), 3269–3282. <https://doi.org/10.1101/gad.1496506>.
- Gahlmann, A., & Moerner, W. E. (2014). Exploring bacterial cell biology with single-molecule tracking and super-resolution imaging. *Nature Reviews. Microbiology*, 12(1), 9–22. <https://doi.org/10.1038/nrmicro3154>.
- Gahlmann, A., Ptacin, J. L., Grover, G., Quirin, S., von Diezmann, L., Lee, M. K., et al. (2013). Quantitative multicolor subdiffraction imaging of bacterial protein Ultrastructures in three dimensions. *Nano Letters*, 13(3), 987–993. <https://doi.org/10.1021/nl304071h>.
- Gómez-García, P. A., Garbaciak, E. T., Otterstrom, J. J., Garcia-Parajo, M. F., & Lakadamyali, M. (2018). Excitation-multiplexed multicolor superresolution imaging with fim-STORM and fim-DNA-PAINT. *Proceedings of the National Academy of Sciences*, 115(51), 12991–12996. <https://doi.org/10.1073/pnas.1804725115>.
- Gustafsson, M. G. L. (2000). Surpassing the lateral resolution limit by a factor of two using structured illumination microscopy. *Journal of Microscopy*, 198(2), 82–87. <https://doi.org/10.1046/j.1365-2818.2000.00710.x>.
- Gustafsson, M. G. L., Shao, L., Carlton, P. M., Wang, C. J. R., Golubovskaya, I. N., Cande, W. Z., et al. (2008). Three-dimensional resolution doubling in wide-field fluorescence microscopy by structured illumination. *Biophysical Journal*, 94(12), 4957–4970. <https://doi.org/10.1529/biophysj.107.120345>.
- Hagen, W. J. H., Wan, W., & Briggs, J. A. G. (2017). Implementation of a cryo-electron tomography tilt-scheme optimized for high resolution subtomogram averaging. *Journal of Structural Biology*, 197(2), 191–198. <https://doi.org/10.1016/j.jsb.2016.06.007>.
- Hammond, L. R., White, M. L., & Eswara, P. J. (2019). γ IVA la DivIVA! *Journal of Bacteriology*, 201(21). <https://doi.org/10.1128/JB.00245-19>. e00245-19.
- Harry, E. J., & Lewis, P. J. (2003). Early targeting of min proteins to the cell poles in germinated spores of *Bacillus subtilis*: Evidence for division apparatus-independent recruitment of min proteins to the division site. *Molecular Microbiology*, 47(1), 37–48. <https://doi.org/10.1046/j.1365-2958.2003.03253.x>.
- Heintzmann, R., & Cremer, C. G. (1999). Laterally modulated excitation microscopy: Improvement of resolution by using a diffraction grating. *Optics Letters*, 24(12), 185–196. <https://doi.org/10.1117/12.336833>.
- Hell, S. W., & Wichmann, J. (1994). Breaking the diffraction resolution limit by stimulated emission: Stimulated-emission-depletion fluorescence microscopy. *Optics Letters*, 19(11), 780–782. <https://doi.org/10.1364/ol.19.000780>.
- Hess, S. T., Girirajan, T. P. K., & Mason, M. D. (2006). Ultra-high resolution imaging by fluorescence Photoactivation localization microscopy. *Biophysical Journal*, 91(11), 4258–4272. <https://doi.org/10.1529/biophysj.106.091116>.
- Himes, B. A., & Zhang, P. (2018). emClarity: Software for high-resolution cryo-electron tomography and subtomogram averaging. *Nature Methods*, 15(11), 955–961. <https://doi.org/10.1038/s41592-018-0167-z>.
- Hsieh, C., Schmelzer, T., Kishchenko, G., Wagenknecht, T., & Marko, M. (2014). Practical workflow for cryo focused-ion-beam milling of tissues and cells for cryo-TEM tomography. *Journal of Structural Biology*, 185(1), 32–41. <https://doi.org/10.1016/j.jsb.2013.10.019>.
- Hu, L., Vecchiarelli, A. G., Mizuuchi, K., Neuman, K. C., & Liu, J. (2017). Brownian ratchet mechanisms of ParA-mediated partitioning. *Plasmid*, 92, 12–16. <https://doi.org/10.1016/j.plasmid.2017.05.002>.

- Hu, J., Worrall, L. J., Hong, C., Vuckovic, M., Atkinson, C. E., Caveney, N., et al. (2018). Cryo-EM analysis of the T3S injectisome reveals the structure of the needle and open secretin. *Nature Communications*, 9, 3840. <https://doi.org/10.1038/s41467-018-06298-8>.
- Huang, B., Jones, S. A., Brandenburg, B., & Zhuang, X. (2008). Whole-cell 3D STORM reveals interactions between cellular structures with nanometer-scale resolution. *Nature Methods*, 5(12), 1047–1052. <https://doi.org/10.1038/nmeth.1274>.
- Huang, B., Wang, W., Bates, M., & Zhuang, X. (2008). Three-dimensional super-resolution imaging by stochastic optical reconstruction microscopy. *Science (New York, N.Y.)*, 319(5864), 810–813. <https://doi.org/10.1126/science.1153529>.
- Jumper, J., Evans, R., Pritzel, A., Green, T., Figurnov, M., Ronneberger, O., et al. (2021). Highly accurate protein structure prediction with AlphaFold. *Nature*, 596(7873), 583–589. <https://doi.org/10.1038/s41586-021-03819-2>.
- Kaplan, M., Oikonomou, C. M., Wood, C. R., Chreifi, G., Ghosal, D., Dobro, M. J., et al. (2022). Discovery of a novel inner membrane-associated bacterial structure related to the flagellar type III secretion system. *Journal of Bacteriology*, 204(8). <https://doi.org/10.1128/jb.00144-22>. e00144-22.
- Khanna, K., Lopez-Garrido, J., Sugie, J., Pogliano, K., & Villa, E. (2021). Asymmetric localization of the cell division machinery during *Bacillus subtilis* sporulation. *eLife*, 10, e62204. <https://doi.org/10.7554/eLife.62204>.
- Kirshner, H., Aguet, F., Sage, D., & Unser, M. (2013). 3-D PSF fitting for fluorescence microscopy: Implementation and localization application. *Journal of Microscopy*, 249(1), 13–25. <https://doi.org/10.1111/j.1365-2818.2012.03675.x>.
- Kraus, F., Miron, E., Demmerle, J., Chitiashvili, T., Budco, A., Alle, Q., et al. (2017). Quantitative 3D structured illumination microscopy of nuclear structures. *Nature Protocols*, 12(5), 1011–1028. <https://doi.org/10.1038/nprot.2017.020>.
- Lawson, I. (2016). Crafting the microworld: How Robert Hooke constructed knowledge about small things. *Notes and Records: The Royal Society Journal of the History of Science*, 70(1), 23–44. <https://doi.org/10.1098/rsnr.2015.0057>.
- Lenz, P., & Sogaard-Andersen, L. (2011). Temporal and spatial oscillations in bacteria. *Nature Reviews. Microbiology*, 9(8), 565–577. <https://doi.org/10.1038/nrmicro2612>.
- Lim, G. E., Derman, A. I., & Pogliano, J. (2005). Bacterial DNA segregation by dynamic SopA polymers. *Proceedings of the National Academy of Sciences*, 102(49), 17658–17663. <https://doi.org/10.1073/pnas.0507222102>.
- Lim, H. C., Surovtsev, I. V., Beltran, B. G., Huang, F., Bewersdorf, J., & Jacobs-Wagner, C. (2014). Evidence for a DNA-relay mechanism in ParABS-mediated chromosome segregation. *eLife*, 3, e02758. <https://doi.org/10.7554/eLife.02758>.
- Lippincott-Schwartz, J., & Manley, S. (2009). Putting super-resolution fluorescence microscopy to work. *Nature Methods*, 6(1), 21–23. <https://doi.org/10.1038/nmeth.f.233>.
- Mahamid, J., Schampers, R., Persoon, H., Hyman, A. A., Baumeister, W., & Plitzko, J. M. (2015). A focused ion beam milling and lift-out approach for site-specific preparation of frozen-hydrated lamellas from multicellular organisms. *Journal of Structural Biology*, 192(2), 262–269. <https://doi.org/10.1016/j.jsb.2015.07.012>.
- Martinez, M., Chen, W. D., Cova, M. M., Molnár, P., Mageswaran, S. K., Guérin, A., et al. (2022). Rhoptry secretion system structure and priming in *plasmodium falciparum* revealed using in situ cryo-electron tomography. *Nature Microbiology*, 7(8), 1230–1238. <https://doi.org/10.1038/s41564-022-01171-3>.
- Medalia, O., & Geiger, B. (2010). Frontiers of microscopy-based research into cell–matrix adhesions. *Current Opinion in Cell Biology*, 22(5), 659–668. <https://doi.org/10.1016/j.ceb.2010.08.006>.
- Medeiros, J. M., Böck, D., & Pilhofer, M. (2018). Imaging bacteria inside their host by cryo-focused ion beam milling and electron cryotomography. *Current Opinion in Microbiology*, 43, 62–68. <https://doi.org/10.1016/j.mib.2017.12.006>.

- Morise, H., Shimomura, O., Johnson, F. H., & Winant, J. (1974). Intermolecular energy transfer in the bioluminescent system of *Aequorea*. *Biochemistry*, 13(12), 2656–2662. <https://doi.org/10.1021/bi00709a028>.
- Mortensen, K. I., Churchman, L. S., Spudich, J. A., & Flyvbjerg, H. (2010). Optimized localization analysis for single-molecule tracking and super-resolution microscopy. *Nature Methods*, 7(5), 377–381. <https://doi.org/10.1038/nmeth.1447>.
- Muok, A. R., Ortega, D. R., Kurniyati, K., Yang, W., Maschmann, Z. A., Sidi Mabrouk, A., et al. (2020). Atypical chemoreceptor arrays accommodate high membrane curvature. *Nature Communications*, 11, 5763. <https://doi.org/10.1038/s41467-020-19628-6>.
- Nakane, T., Kotecha, A., Sente, A., McMullan, G., Masiulis, S., Brown, P. M. G. E., et al. (2020). Single-particle cryo-EM at atomic resolution. *Nature*, 587(7832), 152–156. <https://doi.org/10.1038/s41586-020-2829-0>.
- Park, D., Lara-Tejero, M., Waxham, M. N., Li, W., Hu, B., Galán, J. E., et al. (2018). Visualization of the type III secretion mediated *Salmonella*–host cell interface using cryo-electron tomography. *eLife*, 7, e39514. <https://doi.org/10.7554/eLife.39514>.
- Pilhofer, M., & Jensen, G. J. (2013). The bacterial cytoskeleton: More than twisted filaments. *Current Opinion in Cell Biology*, 25(1), 125–133. <https://doi.org/10.1016/j.ceb.2012.10.019>.
- Ptacin, J. L., Lee, S. F., Garner, E. C., Toro, E., Eckart, M., Comolli, L. R., et al. (2010). A spindle-like apparatus guides bacterial chromosome segregation. *Nature Cell Biology*, 12(8), 791–798. <https://doi.org/10.1038/ncb2083>.
- Radics, J., Königsmaier, L., & Marlovits, T. C. (2014). Structure of a pathogenic type 3 secretion system in action. *Nature Structural & Molecular Biology*, 21(1), 82–87. <https://doi.org/10.1038/nsmb.2722>.
- Rust, M. J., Bates, M., & Zhuang, X. (2006). Sub-diffraction-limit imaging by stochastic optical reconstruction microscopy (STORM). *Nature Methods*, 3(10), 793–796. <https://doi.org/10.1038/nmeth929>.
- Sartori, A., Gatz, R., Beck, F., Rigort, A., Baumeister, W., & Plitzko, J. M. (2007). Correlative microscopy: Bridging the gap between fluorescence light microscopy and cryo-electron tomography. *Journal of Structural Biology*, 160(2), 135–145. <https://doi.org/10.1016/j.jsb.2007.07.011>.
- Scaramuzza, S., & Castaño-Díez, D. (2021). Step-by-step guide to efficient subtomogram averaging of virus-like particles with dynamo. *PLoS Biology*, 19(8), e3001318. <https://doi.org/10.1371/journal.pbio.3001318>.
- Schaffer, M., Pfeffer, S., Mahamid, J., Kleindiek, S., Laugks, T., Albert, S., et al. (2019). A cryo-FIB lift-out technique enables molecular-resolution cryo-ET within native *Caenorhabditis elegans* tissue. *Nature Methods*, 16(8), 757–762. <https://doi.org/10.1038/s41592-019-0497-5>.
- Schermelleh, L., Carlton, P. M., Haase, S., Shao, L., Winoto, L., Kner, P., et al. (2008). Subdiffraction multicolor imaging of the nuclear periphery with 3D structured illumination microscopy. *Science*, 320(5881), 1332–1336. <https://doi.org/10.1126/science.1156947>.
- Schlimpert, S., Klein, E. A., Briegel, A., Hughes, V., Kahnt, J., Bolte, K., et al. (2012). General protein diffusion barriers create compartments within bacterial cells. *Cell*, 151(6), 1270–1282. <https://doi.org/10.1016/j.cell.2012.10.046>.
- Schnell, U., Dijk, F., Sjollem, K. A., & Giepmans, B. N. G. (2012). Immunolabeling artifacts and the need for live-cell imaging. *Nature Methods*, 9(2), 152–158. <https://doi.org/10.1038/nmeth.1855>.
- Sexton, D. L., Burgold, S., Schertel, A., & Tocheva, E. I. (2022). Super-resolution confocal cryo-CLEM with cryo-FIB milling for *in situ* imaging of *Deinococcus radiodurans*. *Current Research in Structural Biology*, 4, 1–9. <https://doi.org/10.1016/j.crstbi.2021.12.001>.

- Shimomura, O., Johnson, F. H., & Saiga, Y. (1962). Extraction, purification and properties of Aequorin, a bioluminescent protein from the luminous hydromedusan, *Aequorea*. *Journal of Cellular and Comparative Physiology*, 59(3), 223–239. <https://doi.org/10.1002/jcp.1030590302>.
- Small, A., & Stahlheber, S. (2014). Fluorophore localization algorithms for super-resolution microscopy. *Nature Methods*, 11(3), 267–279. <https://doi.org/10.1038/nmeth.2844>.
- Söderström, B., Ruda, A., Widmalm, G., & Daley, D. O. Y. (2020). An OregonGreen488-labelled d-amino acid for visualizing peptidoglycan by super-resolution STED nanoscopy. *Microbiology*, 166(12), 1129–1135. <https://doi.org/10.1099/mic.0.000996>.
- Su, C.-C., Lyu, M., Morgan, C. E., Bolla, J. R., Robinson, C. V., & Yu, E. W. (2021). A “build and retrieve” methodology to simultaneously solve cryo-EM structures of membrane proteins. *Nature Methods*, 18(1), 69–75. <https://doi.org/10.1038/s41592-020-01021-2>.
- Sun, J., Liu, C., Peng, R., Zhang, F.-K., Tong, Z., Liu, S., et al. (2020). Cryo-EM structure of the varicella-zoster virus A-capsid. *Nature Communications*, 11, 4795. <https://doi.org/10.1038/s41467-020-18537-y>.
- Thanbichler, M., & Shapiro, L. (2008). Getting organized—How bacterial cells move proteins and DNA. *Nature Reviews Microbiology*, 6(1), 28–40. <https://doi.org/10.1038/nrmicro1795>.
- Turkowsky, B., Schreiber, S., Wörtz, J., Segal, E. S., Mevarech, M., Duggin, I. G., et al. (2020). Establishing live-cell single-molecule localization microscopy imaging and single-particle tracking in the archaeon *Haloflex volcanii*. *Frontiers in Microbiology*, 11. <https://www.frontiersin.org/articles/10.3389/fmicb.2020.583010>.
- von Kügelgen, A., Tang, H., Hardy, G. G., Kureisaite-Ciziene, D., Brun, Y. V., Stansfeld, P. J., et al. (2020). *In situ* structure of an intact lipopolysaccharide-bound bacterial surface layer. *Cell*, 180(2), 348–358.e15. <https://doi.org/10.1016/j.cell.2019.12.006>.
- Kügelgen, A.v., Dorst, S.v., Yamashita, K., Sexton, D. L., Tocheva, E. I., Murshudov, G., et al. (2022). Interdigitated immunoglobulin arrays form the hyperstable surface layer of the extremophilic bacterium *Deinococcus radiodurans*. *bioRxiv*. <https://doi.org/10.1101/2022.09.15.508085>.
- Whelan, D. R., & Bell, T. D. M. (2015). Image artifacts in single molecule localization microscopy: Why optimization of sample preparation protocols matters. *Scientific Reports*, 5(1). <https://doi.org/10.1038/srep07924>. article 1.
- Yang, W., Cassidy, C. K., Ames, P., Diebolder, C. A., Schulten, K., Luthey-Schulten, Z., et al. (2019). *In situ* conformational changes of the *Escherichia coli* serine chemoreceptor in different signaling states. *MBio*, 10(4), e00973–19. <https://doi.org/10.1128/mBio.00973-19>.
- Yuan, S., Wang, J., Zhu, D., Wang, N., Gao, Q., Chen, W., et al. (2018). Cryo-EM structure of a herpesvirus capsid at 3.1 Å. *Science*, 360(6384). <https://doi.org/10.1126/science.aao7283>. eao7283.
- Zachs, T., Schertel, A., Medeiros, J., Weiss, G. L., Hugener, J., Matos, J., et al. (2020). Fully automated, sequential focused ion beam milling for cryo-electron tomography. *eLife*, 9, e52286. <https://doi.org/10.7554/eLife.52286>.